PHYSICAL REVIEW D **94,** 025027 (2016)

Solving functional flow equations with pseudospectral methods

J. Borchardt[*] and B. Knorr[†]

Theoretisch-Physikalisches Institut, Universität Jena, Max-Wien-Platz 1, 07743 Jena, Germany

(Received 5 April 2016; published 20 July 2016)

We apply pseudospectral methods to integrate functional flow equations with high accuracy, extending earlier work on functional fixed point equations [J. Borchardt and B. Knorr, Phys. Rev. D **91**, 105011 (2015)]. The advantages of our method are illustrated with the help of two classes of models: first, to make contact with literature, we investigate flows of the O(N) model in three dimensions, for $N = 1, 4$ and in the large N limit. For the case of a fractal dimension, $d = 2.4$, and $N = 1$, we follow the flow along a separatrix from a multicritical fixed point to the Wilson-Fisher fixed point over almost 13 orders of magnitude. As a second example, we consider flows of bounded quantum-mechanical potentials, which can be considered as a toy model for Higgs inflation. Such flows pose substantial numerical difficulties, and represent a perfect test bed to exemplify the power of pseudospectral methods.

DOI: 10.1103/PhysRevD.94.025027

I. INTRODUCTION

A lot of fundamental problems in particle physics, many-body systems, or even the quantization of gravity arise in situations where coupling constants can grow large. Standard methods as perturbation theory fail to describe these cases, as they are based on an expansion in powers of a small quantity. As not every theory can be simulated straightforwardly by means of discretization, we shall follow another path here, namely the functional renormalization group (FRG), which is a continuum method based on the Wilsonian idea of integrating out momentum modes successively. In particular, this work makes use of the formulation of the exact renormalization group by Wetterich [1], which has been applied to a wide range of systems, e.g., scalar field theories [2–15], fermionic systems [16–22], critical phenomena [23–29], gauge theories [30–37], and quantum gravity [38–58].

Technically, when applying the FRG to a given theory, one has to solve a coupled system of nonlinear (in general integro) differential equations. Only a few cases are known where one can find analytic solutions. In all other cases, the system is considered in a subspace of the space spanned by all operators allowed by symmetry, and the resulting equations are then solved numerically.

Plenty of information can already be retrieved from the fixed point structure of the theory. As an example, the fixed point structure in a condensed matter system may characterize the phase diagram, and the eigenvalues of the perturbations around the fixed points give the critical exponents, controlling, e.g., the scaling behavior near phase transitions. We recently put forward a method to numerically tackle functional fixed point equations globally and with very high precision [59].

Not all questions can be answered by studying fixed points alone. The full functional flows need to be solved, e.g., in regions of physical interest when all couplings run fast, or for the analysis of first order phase transitions. In this work, we extend the ideas of [59] to solve flow equations with the help of pseudospectral methods. In order to benchmark our method, we investigate models which are well understood or widely studied in the FRG context, or can also be controlled by other techniques. First, we study flows of the O(N) model in various dimensions and near as well as away from criticality. Then we investigate quantum mechanical examples with bounded or nonanalytic potentials, as exact results from directly solving the Schrödinger equation can be calculated and compared to. Further applications of the method can be found in [60,61].

We emphasize that the methods presented here are heavily used in other contexts [62,63], as, e.g., finding solutions to Einstein's equation [64,65]. First applications to FRG problems have been given in [66–70]. Additionally, let us point out that full functional flows were already solved in the past employing finite element or finite difference methods [3,71–85].

This paper is organized as follows: in Sec. II, we review some aspects of pseudospectral methods and apply them to study concrete functional flow equations. Then, Sec. III gives a short overview of the FRG, including the truncation and the resulting flow equations that we solve. Consequently, Sec. IV deals with interesting flows of the O(N) model, especially for large N, $N = 1$, and $N = 4$ in $d = 3$ or $d = 2.4$ dimensions. Afterwards, Sec. V discusses both analytical and numerical results on three quantum mechanical potentials which are bounded both from below and above. Finally, Sec. VI contains a short summary.

All numerical results presented here were obtained with C++ code, using the libraries BOOST [86], EIGEN [87], and BLITZ [88], and the 80-bit data type "long double."

[*]julia.borchardt@uni-jena.de
[†]benjamin.knorr@uni-jena.de

II. PSEUDOSPECTRAL METHODS AND THEIR IMPLEMENTATION

This section elucidates the advantages of pseudospectral methods, and how we apply them to solve flow equations. Pseudospectral methods in general are based on orthogonal polynomials. We will focus on Chebyshev polynomials of the first kind here, which are defined by

$$T_n(\cos(x)) = \cos(nx), \tag{1}$$

for all natural numbers n.

A given well-behaved function f, defined on the interval $[a, b]$, can thus be expanded as

$$f(x) = \sum_{i=0}^{\infty} a_i T_i\left(2\frac{x-a}{b-a} - 1\right). \tag{2}$$

In comparison to other orthogonal polynomials, such as Hermite or Laguerre polynomials, Chebyshev polynomials are defined on a finite interval $[-1, 1]$. Both Laguerre and Hermite polynomials are ill suited for our problems since the asymptotic behavior of the expanded function $f(x)$ would depend on the order of expansion. However, the asymptotic behavior of $f(x)$ is fixed.

The usefulness of Chebyshev polynomials in general is (at least) threefold:

(i) the convergence properties depend on the singularity structure of the function: for analytic functions, an expansion in Chebyshev polynomials converges exponentially fast,
(ii) evaluations of the interpolant at any point are easily accessible (by the Clenshaw algorithm) and derivatives of the function are also computable with a minimum amount of effort (similar to the Clenshaw algorithm),
(iii) the highest retained coefficient in an approximation provides a good error estimate for the accuracy of such an expansion.

Of course, there are other sets of basis functions defined on a bounded interval, such as Legendre polynomials, which also show exponential convergence. Nonetheless, there are indications that Chebyshev polynomials converge better, see for example [89].

More details on all of these points are collected in [59], a general overview of Chebyshev polynomials can be found in, e.g., [62].

For the remainder of this section, let us consider a partial differential equation (PDE) of one function f in two variables,

$$\mathcal{L}[f(x, t)] = 0, \tag{3}$$

where $x \in I_x$ and $t \in I_t$ with I_x, $I_t \subseteq \mathbb{R}$, and $\mathcal{L}$ denotes an in general nonlinear (pseudo)differential operator. In the case of flows of the O(N) model, we specialize $I_x = [0, x_{\max}]$ because no boundary effects occur. By contrast, if the potential is bounded as in Sec. V, boundary effects emerge which can only be avoided by taking the function f on the whole positive axis $I_x = [0, \infty)$ into consideration. In particular, we will compactify in the x direction [90]. The specific form of the compactification that we employ is

$$\bar{x} = \frac{x}{1+x}. \tag{4}$$

Although not used here, it is worth mentioning that for unbounded functions which grow like x^n for $x \to \infty$, it is useful to compactify as

$$\bar{f} = \frac{f}{(1+x)^n}. \tag{5}$$

These transformations in combination have the special virtue that they map polynomials to polynomials: for example, if

$$f(x, t) = \sum_{n=0}^{N_x} a_n(t) x^n, \tag{6}$$

after transformation to the new coordinates, we have

$$\begin{aligned}\bar{f}(\bar{x}, t) &= \frac{1}{(1+\frac{\bar{x}}{1-\bar{x}})^{N_x}} \sum_{n=0}^{N_x} a_n(t)\left(\frac{\bar{x}}{1-\bar{x}}\right)^n \\ &= \sum_{n=0}^{N_x} a_n(t)\bar{x}^n(1-\bar{x})^{N_x-n},\end{aligned} \tag{7}$$

which is polynomial in $\bar{x}$. For the sake of readability, from now on we will drop any bar on transformed quantities when there is no danger of confusion.

Let us make a short comment on why we use pseudospectral methods also in the time direction. There are also *Ansätze* combining pseudospectral methods in the field direction with a standard ordinary differential equation solver, such as Runge-Kutta, for the time direction. We have decided on a pseudospectral treatment of both directions to achieve as much accuracy as possible. This is especially important for fine-tuning problems and flows over many orders of magnitude to obtain reliable results [61].

To obtain high efficiency and better convergence, it is useful to decompose the x and t domain of definition into subdomains. This is illustrated in Fig. 1. The PDE is solved simultaneously on all x subdomains of a specific t slice $t \in [t_i, t_{i+1}]$. Imposing the initial condition on the first slice and continuity on the following slices leads to an initial value problem on every time patch. For that purpose, we expand the (potentially compactified) function f on every t slice (mapped to $[-1, 1]$), in every (compactified) x subdomain (also mapped to $[-1, 1]$) as a tensor product,

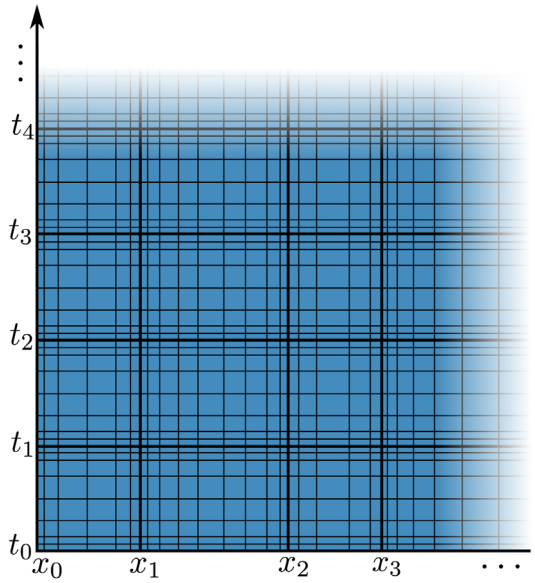

FIG. 1. Sketch on the decomposition of the domain of definition into subdomains. t_i and x_i denote the boundaries of the subdomains in the t and x directions, respectively. For each subdomain an own expansion of f is used. The thin grid lines depict the Chebyshev grid for each subdomain.

$$f(x,t) = \sum_{i=0}^{N_x} \sum_{j=0}^{N_t} a_{ij} T_i(x) T_j(t). \tag{8}$$

This *Ansatz* can be inserted into the PDE. To solve for the coefficients a_{ij}, we employ the collocation method, where the PDE is evaluated at a set of collocation points and the subsequent algebraic, nonlinear system of equations is solved by a stabilized Newton-Raphson iteration. For the collocation method to work so well, the essential point is the specification of the grid. The most common choices are Gauss, Lobatto, and one-sided Radau grids [91]. All of them share their nonuniform density of grid points, and are equally suited regarding convergence properties.

As collocation points, we specify a one-sided Radau grid in the t direction, including the end point of the patch, and a Gauss grid on all x subdomains. As already mentioned, one has to match the initial condition in the t direction as well as the function value and a certain number of derivatives at the boundaries of the subdomains in the x direction. The exact number of conditions is dictated by the order of the differential equation: if the order is p, then $p-1$ derivatives have to be matched. From this, our specific choice of the grid becomes clearer. Using a Lobatto or Radau grid in the x direction may lead to instabilities, when in addition to the matching conditions, the PDEs are demanded at the boundary points. In order to avoid potential problems, we consequently use a Gauss grid. For the t direction, the situation is slightly different. There, one solves an initial value problem, thus it may be better not to use a left-sided Radau or Lobatto grid, as they include the initial time slice, which might lead to an overdetermination. Using a right-sided Radau grid is practical in the sense that one already has the values of the function on the final time slice, and does not need to calculate them from the solution of the time patch in order to get the initial condition for the next patch.

Lastly, let us remark that a generalization to multiple functions is straightforward by introducing a tensor product expansion for any given function. In the context of specific truncations, one may additionally deal with functions that do not depend on x, such as single running couplings. These are naturally incorporated by taking $N_x = 0$.

III. FUNCTIONAL RENORMALIZATION GROUP

The functional renormalization group is a nonperturbative tool for successively integrating out quantum fluctuations in a controlled way. For this, an effective average action Γ_k is introduced which smoothly connects the microscopic action $\Gamma_\Lambda = S_{\rm cl}$ at the ultraviolet (UV) cutoff Λ and the macroscopic action $\Gamma_0 = \Gamma$. This flow is described by the Wetterich equation [1],

$$\partial_t \Gamma_k = \frac{1}{2} \mathrm{STr}[(\Gamma_k^{(2)} + R_k)^{-1} (\partial_t R_k)], \qquad t = \log\left(\frac{k}{\Lambda}\right), \tag{9}$$

that is an exact functional, integro-differential equation. Here, $\Gamma_k^{(2)}$ denotes the second functional derivative of Γ_k with respect to the fields and the supertrace STr stands for summation (integration) over discrete (continuous) indices and provides a minus sign for Grassmann-valued fields, i.e. fermions. The regulator function R_k prevents the flow from divergencies both in the UV and the infrared (IR). For more information on the FRG, we refer the reader to, e.g., [3,4,23,31,32].

The common case is that Eq. (9) can only be solved within a certain truncation of the effective average action. A systematic expansion is provided by the derivative expansion. The systems we consider in what follows go all back to the same *Ansatz* for the effective average action,

$$\Gamma_k[\sigma] = \int \mathrm{d}^d x \left\{ \frac{1}{2} Z(\partial_\mu \sigma^a)(\partial^\mu \sigma^a) + U(\sigma^a \sigma^a / 2) \right\}. \tag{10}$$

Within the local potential approximation (LPA or LPA′), the full field and scale dependence of the effective potential U is retained. The wave function renormalization Z is field independent, and is therefore only a function of the scale k (LPA′) or constant during the flow (LPA). In Sec. IV the index of the bosonic scalar field σ counts the N different components. When we consider quantum-mechanical systems in Sec. V, σ stands for the position x, and the index counts the space dimensions. Also, the integration and differentiation in the action are with respect to the

Euclidean time coordinate, $\mathrm{d}x \equiv \mathrm{d}\tau$. In both cases the invariant ρ is given by $\rho = \sigma^a\sigma^a/2$.

IV. FLOWS OF THE O(N) MODEL

The O(N)-symmetric model is a relevant model for many aspects of particle physics, condensed matter systems, and QCD. It consists of bosonic fields only, exhibits a global symmetry, there is an analytical solution for the large N limit (see [2,92] for approaches using the Wetterich equation), and the $N = 1$ case is even exactly solvable in $d = 1$ [93] and $d = 2$ [94]. Additionally, it provides physically interesting features for $d < 4$, such as a rich fixed point structure. Therefore, it is a good testing ground for demonstrating properties of pseudospectral methods.

The flow of the first derivative of the potential with respect to the field is numerically more stable than the flow of the potential itself [95]. Therefore, we employ the flow equation for the dimensionless quantities $u'(\tilde{\rho}) = \partial_{\tilde{\rho}} u(\tilde{\rho})$ [2] where $\tilde{\rho} = Zk^{2-d}\rho$ and $u = U/k^d$,

$$\begin{aligned}\partial_t u'(\tilde{\rho}) &= (-2+\eta)u'(\tilde{\rho}) + (d-2+\eta)\tilde{\rho}u''(\tilde{\rho}) \\ &\quad - \frac{4v_d}{d}\left(1-\frac{\eta}{d+2}\right) \\ &\quad \times \left(\frac{3u''(\tilde{\rho}) + 2\tilde{\rho}u'''(\tilde{\rho})}{(1+u'(\tilde{\rho})+2\tilde{\rho}u''(\tilde{\rho}))^2} + \frac{(N-1)u''(\tilde{\rho})}{(1+u'(\tilde{\rho}))^2}\right).\end{aligned} \tag{11}$$

Here, $v_d^{-1} = 2^{d+1}\pi^{d/2}\Gamma(d/2)$, and the anomalous dimension is defined as $\eta = \partial_t \ln Z$, and given by [96]

$$\eta = \frac{16v_d}{d}\frac{\tilde{\rho}_0 u''(\tilde{\rho}_0)^2}{(1+2\tilde{\rho}_0 u''(\tilde{\rho}_0))^2}, \tag{12}$$

evaluated at the vacuum expectation value (vev) $\tilde{\rho}_0$. For the regularization the linear optimized regulator is employed [97], $R_k(p^2) = Z(k^2 - p^2)\theta(k^2 - p^2)$. For aspects of optimization, see also [98]. In the first part of this section we set $\eta \equiv 0$ ($Z \equiv 1$), which becomes exact for a large N. In the last part, we take the scale dependence of the wave function renormalization into account.

A. Flows for $d = 3$ and at large N: A comparison

In order to demonstrate the power of pseudospectral methods on a specific example, we compare the analytical flow for a large N with the numerically computed one. For that purpose, we choose trajectories in the symmetry broken phase close to criticality to show stability of the numerical method for 6 orders of magnitude ($t \in [0, -12.4]$). We use (11) in the limit $N \to \infty$ [92] (where one only retains the scaling part and the fluctuation part proportional to N) and switch to dimensional quantities as soon as the vev starts scaling exponentially in t. We expand the first derivative of the potential on [0, 0.2] for the dimensionless and on $[0, 0.2k_S]$ for the dimensional flow, where k_S is the scale of switching between both regimes. With this choice, the maximal field value is 10–20 times larger than the vev. In general, the field range must not be too small in order to avoid boundary effects.

The initial condition reads

$$U'_\Lambda(\rho) = -0.008443603515625 + 0.5\rho \tag{13}$$

at $t = 0$ or $k = \Lambda$, where Λ is the UV cutoff. All dimensional quantities are to be understood in units of Λ, which we set to 1. For switching to the dimensional version of (11), we choose $t_s = \ln(k_S/\Lambda) = -10.1$. Furthermore, the temporal subdomains and N_t are taken to achieve exponential convergence down to machine precision in this direction. In order to compare the analytical potential [92] with the numerically computed one, we employ the maximum norm of their difference as an error criterion.

In Fig. 2 the absolute deviation of the numerical flow from the analytical one in dependence on the number of the coefficients N_x in the field direction can be seen. The flow was compared at two scales: $t = -10$ ($k = 4.5 \times 10^{-5}$), before switching to dimensional quantities, and $k = 4 \times 10^{-6}$ ($t = -12.4$), after switching to dimensional quantities, where we have stopped the integration. We also depict the relative error of the vev at this scale. The more coefficients taken into account, the higher the accuracy, which can be seen by the exponential convergence of $\delta U'(\rho)$ and $\delta\rho_0/\rho_0$ in particular. For the error $\delta u'(\tilde{\rho})$ at $t = -10$ we see a plateau for $N_x \gtrsim 60$. This can be explained by the condition of the differential equation. To illustrate this, we compare two analytically computed solutions, one with the initial condition (13), and the other

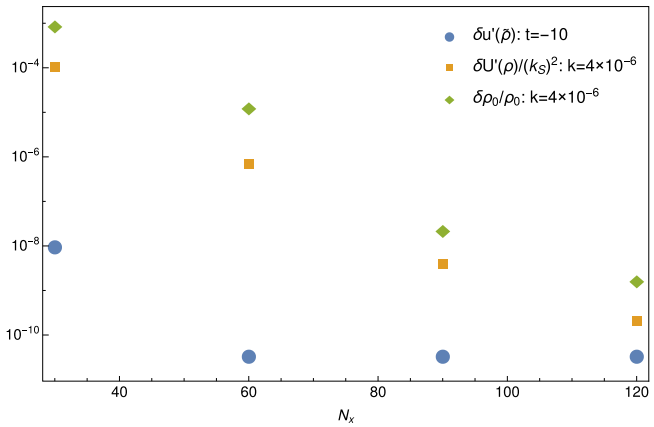

FIG. 2. Absolute and relative error [$\delta u'(\tilde{\rho})$, $\delta U'(\rho)$ and $\delta\rho_0/\rho_0$] of the first derivative of the potential and the vev, respectively, as a function of the number of coefficients N_x in the field direction. The errors $\delta U'(\rho)$ and $\delta\rho_0/\rho_0$ decrease exponentially. For the error of $u'(\tilde{\rho})$ at $t = -10$, one can see a plateau which is due to the condition of the differential equation. This indicates that the solution is accurate to almost machine precision.

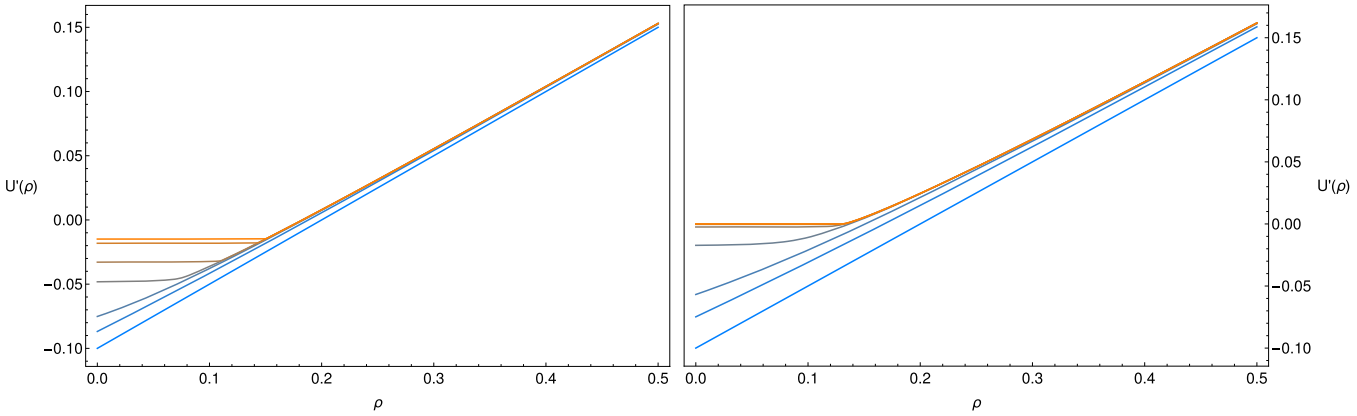

FIG. 3. Evolution of $U'(\rho)$ from blue (bottom) to orange (top) for $N = 1$ (left panel; $t = 0, -0.5, -1, -1.5, -1.7, -2, -2.1$) and $N = 4$ (right panel; $t = 0, -0.5, -1, -2, -3, -4, -5, -13$). Convexity is seen in the flattening of $U'(\rho)$ for small fields $\rho < \rho_0$. Whereas $U''(\rho)$ is still continuous for $N = 4$, in the single scalar case a jump occurs.

with a small deviation from it. To obtain an error of about $\sim 10^{-11}$ at $t = -10$, one can allow for a deviation of 10^{-18} for the constant term, and 10^{-16} for the linear term, which is about the order of magnitude that we can resolve with long double. This example indicates how carefully time integration has to be done for staying close to the original trajectory. On the other hand, it shows that we have integrated out the flow close to machine precision over many orders of magnitude for $N_x \gtrsim 60$. This fact is supported by the exponential convergence till $\sim 10^{-18}$ of the coefficients.

For the IR flow, the decrease of the error is slower, but still tends to the lower bound $\sim 10^{-11}$ for a large number of coefficients. The error is now dominated by the truncation error of the expansion of the potential in field direction since convexity starts to set in. From the asymptotic decrease of the last coefficients for $N_x \gtrsim 60$, we obtain a measure for the truncation error which agrees very well with the errors depicted in Fig. 2. It is based on an estimate for the sum over the neglected coefficients. In order to achieve machine precision, more coefficients are needed.

We conclude that in a large part of theory space, the pseudospectral flow is highly efficient, and we generically observe exponential convergence for an increasing number of Chebyshev coefficients. Therefore, we concentrate in the following on the most challenging part of theory space involving the buildup of nonanalyticities, the first adumbration of which we just started to discuss.

B. Flows for $d = 3$ and $N = 1, 4$

In the spontaneously symmetry broken phase, the effective potential is nonconvex for all intermediate scales $k > 0$. On the other hand, it is known that the effective potential has to be convex at $k = 0$ even in the LPA [3,99]. While the outer region already is convex, the inner region becomes flat during the IR flow. Since the radial mass does not vanish for $N = 1$, the curvature jumps at the vev at $k = 0$. By contrast for $N > 1$, the influence of Goldstone bosons partly suppresses this nonanalyticity. The propagators $\propto (1 + u'(\tilde{\rho}))^{-1}$ and $\propto (1 + u'(\tilde{\rho}) + 2\tilde{\rho}u''(\tilde{\rho}))^{-1}$ flow towards the singularity for small $\tilde{\rho}$, pushing the convexity mechanism forward.

We picked out two particular values for N, namely $N = 1$ and $N = 4$. The following calculations are done with the dimensional version of (11) since we choose the initial condition to be far from criticality, $U'_\Lambda(\rho) = -0.1 + 0.5\rho$, at $k = \Lambda$. It is convenient to use the logarithmic time scale t instead of k. After a few orders of magnitude, dimensional scaling can be observed.

Figure 3 depicts the evolution of $U'(\rho)$ for $N = 1$ and $N = 4$, from large to small scales. The approach to convexity is clearly visible. The buildup of the corresponding nonanalyticity can be monitored over a range of scales, especially for $N = 4$. As $U'(\rho)$ for $N = 1$ has an edge at ρ_0 at $k = 0$ where $U''(\rho_0)$ jumps, the flow is numerically much harder to track and finally breaks down earlier. The reason is as follows: exponential convergence of the coefficients is only guaranteed if the function is analytical. For $k = \Lambda$, the convergence of the coefficients in the field direction is very fast. Plateaus that build up for higher order coefficients are on the level of the machine precision. However, for low scales k, the requirement for exponential convergence is not fulfilled anymore. Thus, we observe a slower convergence of the coefficients till it breaks down. Although this problem cannot be avoided completely, there are two possibilities for improvement: on the one hand, one can simply take more coefficients. This will not cure the problem completely since the convergence becomes too slow and finally, an unacceptably large number of coefficients is needed. On the other hand, one can choose the domains in such a way that the nonanalyticity lies close to the boundary of two neighboring domains. For that reason, we have used 24 and 16 domains for $N = 1$ and $N = 4$, respectively. The high accuracy of pseudospectral

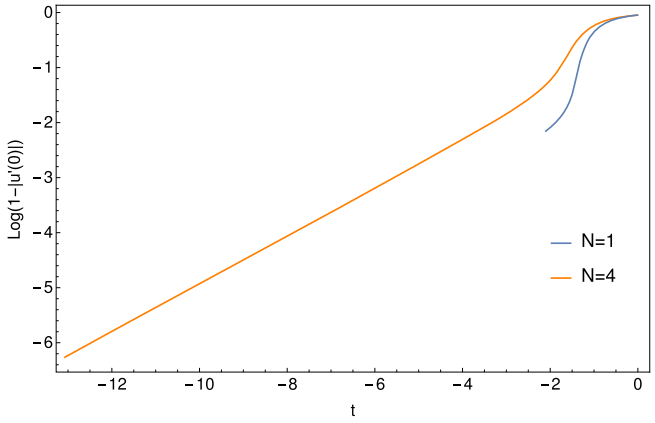

FIG. 4. $u'(0)$ approaches the singularity -1 for $t \to -\infty$. Due to the stronger nonanalyticity in the single scalar case, the numerically computed flow ceases to exist earlier.

methods prevents the flow to jump over the singularity of the propagator for a long time. Figure 4 shows how the flow approaches the singular point. Due to the reasons given above, for $N = 4$ we get closer to $u'(0) = -1$ in comparison to $N = 1$.

We have shown that pseudospectral methods can also be applied to numerically challenging problems, such as convexity. Let us emphasize that the convergence of the expansion coefficients is strongly connected to the properties of the solution. Therefore, it is not surprising that the numerical effort increases the closer the singularity is approached. In contrast to other approaches adjusted to tackle convexity issues [76,85], we again point out that pseudospectral methods have a striking advantage: the error is controllable by the convergence pattern of the expansion coefficients, which was especially demonstrated in the previous section. Furthermore, if only IR quantities are of interest, e.g., the vev, they can be inferred from the flow before convexity becomes challenging. We obtain $\rho_0 = 0.183$ for $N = 1$ and $\rho_0 = 0.130$ for $N = 4$ and the radial mass $m_R^2 = 2\rho_0 U''(\rho_0) = 0.168$ for $N = 1$. It is worth mentioning that the vev for $N = 4$ deviates by 2% from the vev derived from the analytical large N solution. That indicates that the large N limit already is a proper approximation for the $N = 4$ case.

Let us make a comment on first order phase transitions. In contrast to continuous phase transitions, the order parameter, i.e. the vev, jumps. For all quantities whose flow depends on the order parameter, for example the anomalous dimension, one should adapt the domain decomposition in time direction such that the jump is exactly on the boundary between two domains, as was done in [61].

Finally, note that pseudospectral methods are easily extendable to higher truncations, e.g., taking a field-dependent wave function renormalization or p^4 operators into account [60].

C. Flow between two criticalities for $N = 1$

In the previous section, we have investigated flows far from criticality. However, for $d < 4$, nontrivial fixed points occur. The first one is the well-known Wilson-Fisher fixed point. Lowering the dimension further, multicritical fixed points emerge at certain critical dimensions $d_{c,i} = 2i/(i-1)$ for $i \geq 3$. This is discussed in [9,13,100] in detail. In [59] global solutions of the first four fixed point potentials for $d = 2.4$ are given. Now, we take a closer look at the first two fixed points, the Wilson-Fisher fixed point among them, in $d = 2.4$. We are interested in a trajectory connecting both (separatrix). Therefore, we start at the tricritical fixed point with a small deviation constructed from a linear combination of its relevant eigenperturbations. For our calculations we employ (11) and (12) with the wave

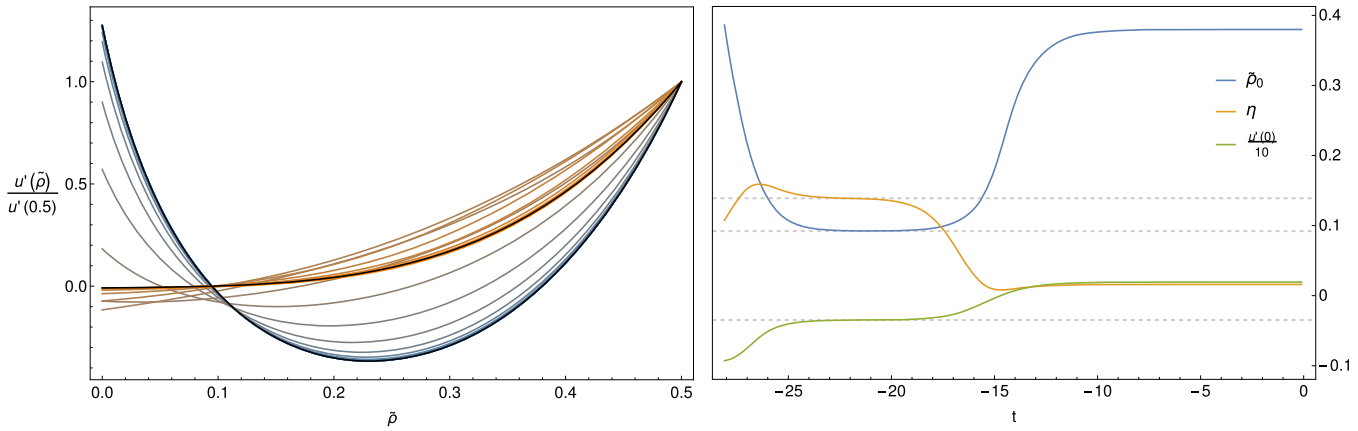

FIG. 5. Flow between two criticalities. (Left panel) Flow from the tricritical fixed point potential (blue) to the Wilson-Fisher potential (orange), $t \in [0, -25]$. The fixed point potential computed from the fixed point equation are depicted as well (black). (Right panel) Flow of the anomalous dimension η, the vev and $u'(0)$. The grey dashed lines denote the values of the Wilson-Fisher fixed point solution obtained from solving the fixed point equation.

function renormalization being scale dependent. As initial conditions we use the results of [59].

For approaching the Wilson-Fisher fixed point during the flow, we have to fine-tune the linear combination of both relevant directions of the tricritical fixed point. The perturbation is mainly along the second relevant (subleading) direction. The flow strongly depends on the numerical parameters. This is not surprising since small perturbations in the relevant direction may lead to large deviations during the flow as already seen for the large N case. Figure 5 shows the deformation of the potential $u'(\tilde{\rho})$ from the tricritical fixed point to the Wilson-Fisher fixed point during the flow. The inner minimum of the tricritical fixed point potential disappears. In the right panel the anomalous dimension, the vev, and $u'(0)$ are plotted over the logarithmic scale. Whereas all quantities and the potential itself stay at the tricritical fixed point for many orders of magnitude, they finally approach the Wilson-Fisher fixed point. This can be seen from the plateaus at $-17 \gtrsim t \gtrsim -25$. The relevant direction becomes irrelevant at the Wilson-Fisher fixed point. Finally, the flow carries the critical behavior of the Wilson-Fisher fixed point although we have started at the tricritical fixed point. We emphasize that for such flows a very stable numerical method is indispensable for which pseudospectral methods are well suited.

V. QUANTUM MECHANICS WITH A BOUNDED POTENTIAL

In this section we present results on the energies of the ground and first excited states of a selection of three quantum-mechanical potentials obtained by solving the flow equation for the derivative of the effective potential. This is specifically suited to test our methods, as a direct comparison with other methods and the exact answer is possible, and in the FRG framework, an extension to quantum field theory is straightforward.

In particular, we will focus on potentials that are bounded from both below and above. Physically, such potentials are interesting, e.g., in the context of Higgs inflation [101]. Technically, the flows of such potentials necessitate a global resolution—if the flow of only a finite region in x is considered, one encounters boundary effects that destabilize the flow. To put the results in perspective, we will compare them with the (numerically) exact values, as well as values obtained from various analytic approximations.

A. Models

We will consider three different potentials. As a first example, we will treat

$$U(x) = \frac{2}{\pi}\arctan(x^2). \tag{14}$$

This potential carries no additional special properties besides the boundedness. We include it, because one can solve the flow in a large N approximation exactly and explicitly for this potential. As a second potential, we choose a modified version of the well-known Pöschl-Teller potential,

$$U(x) = \frac{\lambda(1+\lambda)}{2}\left(1 - \frac{1}{\cosh^2(\lambda x)}\right). \tag{15}$$

For this potential, the Schrödinger equation can be solved exactly, and all bound states and their corresponding energies are known [102]. In this work, we will specify to the case $\lambda = 1$. The Pöschl-Teller potential is also interesting from another point of view: it is reflectionless for $\lambda \in \mathbb{N}$, so waves are transmitted completely through the well. Lastly, we shall investigate the influence of nonanalyticities by studying the potential

$$U(x) = e^{-1/x^2}. \tag{16}$$

All potentials are normalized such that they go to 1 when the argument goes to infinity, and vanish at their minimum $x = 0$.

B. Exact results

Here we present the (partly numerically) exact solutions for the ground state and the first excited state (if it exists) for all potentials by solving the Schrödinger equation (in natural units),

$$-\frac{1}{2}\Psi''(x) + U(x)\Psi(x) = E\Psi(x). \tag{17}$$

For the Pöschl-Teller potential with $\lambda = 1$, there is only one bound state,

$$\Psi_0(x) = \frac{1}{\cosh(x)}, \qquad E_0 = 1/2. \tag{18}$$

For the other potentials, we apply pseudospectral methods along the lines of [59] to obtain the first two bound states. For the potential (14), the ground state energy, E_0, and the energy gap, $\Delta E = E_1 - E_0$, are

$$E_0 = 0.448004, \qquad \Delta E = 0.509453. \tag{19}$$

On the other hand, for the nonanalytic potential (16), we get

$$E_0 = 0.356644, \qquad \Delta E = 0.542040. \tag{20}$$

All energies and their corresponding wave functions were determined with an accuracy of at least 10^{-20}, however there is no need to display more figures in order to discuss all subsequent results.

C. WKB approximation

In order to assess the following results, we compare them with the WKB approximation. The formula for the approximated energy levels reads

$$\int_{-x_0}^{x_0} \sqrt{2(E_n - U(x))} = \left(n + \frac{1}{2}\right)\pi, \tag{21}$$

where x_0 is the classical turning point, $U(x_0) = U(-x_0) = E_n$. The index n counts the energy level. Evaluating (21) for each model, we obtain for the first potential, (14),

$$E_0 \approx 0.520, \qquad E_1 \approx 0.955, \qquad \Delta E \approx 0.435. \tag{22}$$

For the Pöschl-Teller potential, (15), the ground state energy is

$$E_0 \approx 0.582. \tag{23}$$

Finally for the last potential, (16), we have

$$E_0 \approx 0.405, \qquad E_1 \approx 0.905, \qquad \Delta E \approx 0.500. \tag{24}$$

It is remarkable that E_1 deviates less than 1% from the exact value, whereas E_0 is off by 13%–16%. This is to be expected, since the WKB approximation works well in the semiclassical limit $\lambda \ll 2x_0$, where $\lambda/2$ is the distance between two knots of the wave function. This translates into the condition $n \gg 1$.

D. One-loop approximation

As a further step to put subsequent results in perspective, we perform a one-loop calculation. The one-loop effective potential reads

$$U_{\text{1-loop}}(x) = U_{\text{cl}}(x) + \frac{1}{2}\sqrt{U''_{\text{cl}}(x)}, \tag{25}$$

which can for example be obtained directly from the flow equation (9) by setting the potential on the right-hand side equal to the classical potential U_{cl}. The ground state energy is given by the value of the effective potential at its minimum (here in all cases $x = 0$), whereas the energy gap is the square root of the curvature of it, also evaluated at the minimum. One thus obtains for the first potential, (14),

$$E_0 = \frac{1}{\sqrt{\pi}} \approx 0.564, \qquad \Delta E = \frac{2}{\sqrt{\pi}} \approx 1.128. \tag{26}$$

The ground state energy comes out more or less well for such a simple calculation, but the one-loop result predicts that there are no further bound states, as the energy gap is too large.

For the Pöschl-Teller potential, the one-loop result is

$$E_0 = \frac{1}{\sqrt{2}} \approx 0.707, \qquad \Delta E = \sqrt{2(1-\sqrt{2})} \approx 0.910\mathbf{i}. \tag{27}$$

The convexity of the effective potential is not caught by a one-loop calculation, and accordingly, the energy gap is imaginary. This phenomenon is well known to be an artifact of the loop expansion, and extensively discussed in, e.g., [103,104]. The ground state energy is off by about 40%.

Finally, for the nonanalytic potential (16), no meaningful one-loop analysis can be done. In fact, any order in perturbation theory fails to produce anything nonzero for the energy levels because of the nonanalyticity.

E. Flow of the effective potential

This section is devoted to the numerical study of the actual flow equation for the effective potential. All investigations are done within a LPA where $Z \equiv 1$. Note that in quantum mechanics no renormalization is needed. Therefore, the initial condition can be put at $k = \Lambda \to \infty$. To cover the whole interval $k \in [0, \infty)$ the time direction is compactified analogously to (4). As in the previous section, for reasons of numerical stability, we actually use the flow equation for the derivative of the effective potential $U'(\rho) = \partial_\rho U(\rho)$, and obtain the ground state energy by an additional integration. The flow equation reads

$$\partial_k U'(\rho) = -Ak^B \frac{3U''(\rho) + 2\rho U'''(\rho)}{(k^2 + U'(\rho) + 2\rho U''(\rho))^C}, \tag{28}$$

where $A = 1/\pi$, $B = C = 2$ for the linear optimized regulator $[R_k(p^2) = (k^2 - p^2)\theta(k^2 - p^2)]$ and $A = 1/4$, $B = 1$, and $C = 3/2$ for the Callan-Symanzik cutoff $[R_k(p^2) = k^2]$.

We will first point out some expectations on the outcome of the flow, followed by the discussion of the actual results of the flow. An overview of all results can be found in Table I.

1. Expectations

The effective potential needs to be convex at $k = 0$ (except in particular cases, see the discussion in the next section). It is immediately clear that any bounded function that is not constant cannot be convex. It follows that if we could integrate the flow equations down to $k = 0$, we would end up with a constant potential, and the constant is exactly the ground state energy. One can prove this by considering an alternative definition of the effective potential [105],

$$U(\bar{x}) = \inf_{\Psi:\langle x\rangle = \bar{x}} \langle H \rangle, \tag{29}$$

that is, the effective potential at a point $\bar{x}$ is given by the infimum of the Hamiltonian over all states with the position

TABLE I. Overview of exact results from solving the Schrödinger equation and results obtained from the flow of the potential for all three potentials. CS and opt indicate that the Callan-Symanzik and the optimized regulator were employed, respectively.

$V(x) = 2/\pi \arctan(x^2)$			
	Exact	CS	Opt
E_0	0.448004	0.445	0.447
ΔE	0.509453	0.477	0.558
$V(x) = 1 - 1/\cosh^2(x)$			
	Exact	CS	Opt
E_0	1/2	0.496	0.499
ΔE	⋯	0.464	0.585
$V(x) = \exp(-1/x^2)$			
	Exact	CS	Opt
E_0	0.356644	0.355	0.356
ΔE	0.542040	0.515	0.570

expectation value $\bar{x}$. Exhaustive discussions of the effective potential in quantum field theory can be found in, e.g., [105–108]. Our naive expectation on the flow is therefore that we can hope to find the ground state energy, but probably not the energy of the first excited state. Surprisingly, it turns out that one can extract some estimate of the excited state energy from the flow.

2. Numerical results

As an exemplary case, we display the numerical results from solving the flow equation for the nonanalytical potential (16). The other two potentials pose no further challenges and show the same qualitative behavior.

In Fig. 6, the effective potential at $x = 0$ as a function of the scale k is depicted, for both the Callan-Symanzik and the optimized regulator. It corresponds to the effective ground state energy at scale k. The horizontal dashed line indicates the exact value obtained from the Schrödinger equation. For technical reasons, we cannot integrate down to $k = 0$, but only to a finite value, indicated by the vertical dashed line. From there on, we extrapolate linearly to get an estimate of the true ground state energy. For both regulators, we get very precise estimates for the ground state energy. Generically, the optimized regulator gives slightly superior results for E_0.

Next, we shall discuss the results on the energy gap. As argued above, in principle we should not expect to get any meaningful estimate from the effective potential. There is however a loophole in the above argument: it is based on the effective potential at scale $k = 0$, when all fluctuations are integrated out. When we consider the flow of the effective potential, we can extract further information, as the scale k is roughly the (inverse) scale of a finite box that the system lives in, giving an effective cutoff to the physics. In this sense, we can indeed extract information on the energy gap, roughly when the scale is large enough to resolve the wave function of the first excited state, but small enough not to be too strongly influenced by the next-higher states. Bearing this in mind, we shall discuss the first derivative of the flowing potential, again at vanishing position, which gives the effective energy gap at scale k [109],

$$\Delta E = \sqrt{U'(\rho)}|_{\rho=0}. \tag{30}$$

It is shown in Fig. 7, again for both regulators. Remarkably, in both cases again, we get quite a good estimate of the true energy gap, however the finer details are more complicated. For the Callan-Symanzik regulator, we can already see the

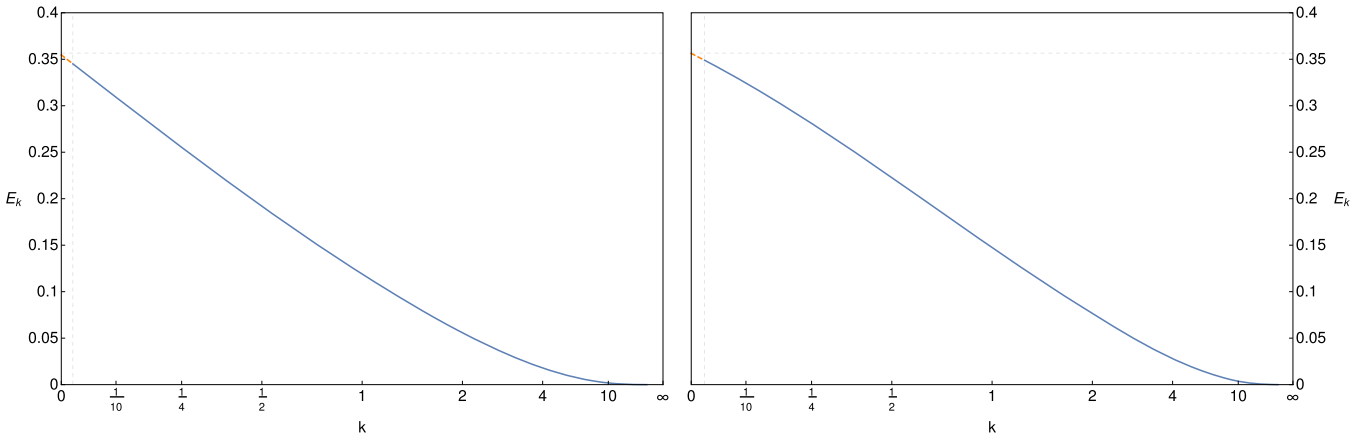

FIG. 6. Flow of the effective potential at vanishing position, which gives the effective ground state energy at scale k, E_k, for both the Callan-Symanzik (left panel) and the optimized (right panel) regulator. The horizontal dashed line indicates the exact value of the ground state energy, whereas the vertical line indicates the value up to which the numerical integration could be done. The orange dashed line is the extrapolation of our numerical values, given in blue. In both cases, the ground state energy is obtained at surprisingly high accuracy.

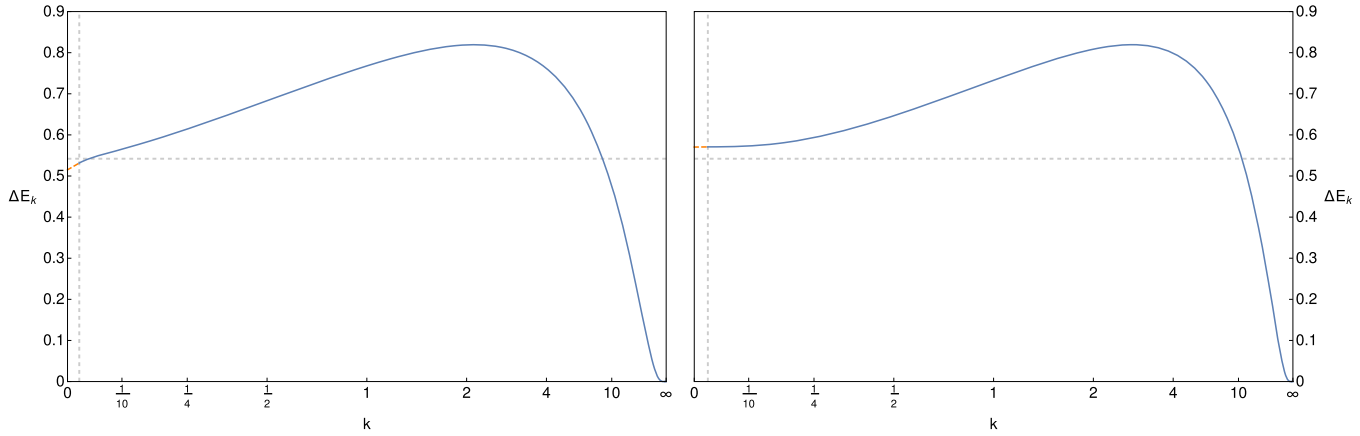

FIG. 7. Flow of the derivative of the effective potential at vanishing position, which gives the effective energy gap at scale k, ΔE_k, for both the Callan-Symanzik (left panel) and the optimized (right panel) regulator. The horizontal dashed line indicates the exact value of the energy gap, whereas the vertical line indicates the value up to which the numerical integration could be done. The orange dashed line is the extrapolation of our numerical values, given in blue. The energy gap comes out quite well in both cases.

influence of convexity, as the derivative of the effective potential bends towards zero. This is not the case for the optimized regulator yet. Correspondingly, the optimized regulator overestimates the energy gap, whereas the estimate from the Callan-Symanzik regulator is below the true value. This behavior is also observed for the other potentials, and influences the prediction of the number of bound states. In this respect, the optimized regulator erroneously predicts only one bound state for the potential (14). On the other hand, the Callan-Symanzik regulator predicts a second bound state for the Pöschl-Teller potential (15). Either way, any prediction for the energy gap from the flow should be taken with a grain of salt, as convexity has to set in at some point, and also the extrapolation introduces further errors. Presumably one should read off the energy gap at some finite value of the scale, at which the first excited state is completely resolved, however we found no *a priori* argument on how to set this scale.

In Fig. 8, we depict the actual flow of the derivative of the effective potential, obtained with the Callan-Symanzik regulator. One can see that the nonanalyticity of the classical potential is smoothed out quickly. For small scales k, one can also see the tendency of the derivative of the effective potential to flow to zero, as it must due to convexity. In contrast to unbounded potentials, where convexity is numerically challenging near the origin, the numerical problems here arise for large values of the position, which makes it increasingly difficult to resolve the flow.

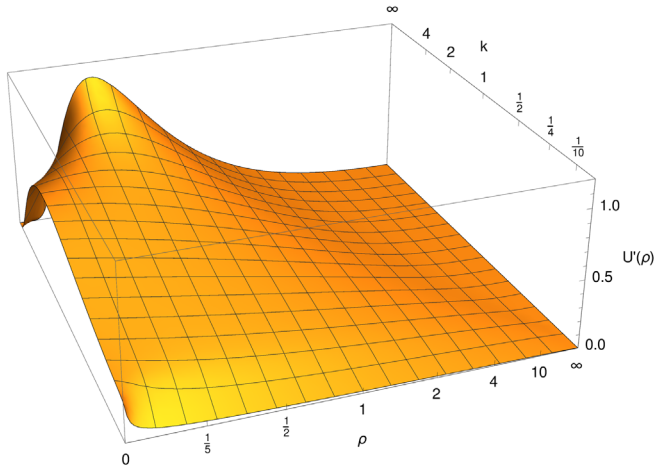

FIG. 8. Flow of the derivative of the effective potential for the Callan-Symanzik regulator. One can see that the nonanalyticity of the classical potential quickly smooths out. Convexity problems for small scales arise for large values of the position, in contrast to conventional unbounded potentials.

F. Large N approximation

As a final point, we shall study the potential (14) in the limit of infinitely many dimensions, similar to a large N approximation in the O(N) model. This means specifically that the index a in (10) counts the space coordinates, and we allow it to run from 1 to N, sending $N \to \infty$. In this case, the flow equation can be solved implicitly by the method of characteristics [92]. In the case of the potential (14), the implicit relation $x = x(U)$ can be inverted, delivering the full effective potential. It is given by

$$U(x) = \frac{-\pi x^2 + \sqrt{16\pi(1+x^4) - \pi^2}}{8\pi(1+x^4)} + \frac{2}{\pi}\left(\arctan(x^2) + \arctan\left(\sqrt{\frac{\pi}{16(1+x^4)-\pi}}\right)\right). \tag{31}$$

Notably, the large N effective potential is *not* convex. This seeming paradox has the following reason. Convexity is tied to the condition that the propagator avoids a singularity for negative $U''(x)$ which appears in the equivalent of the

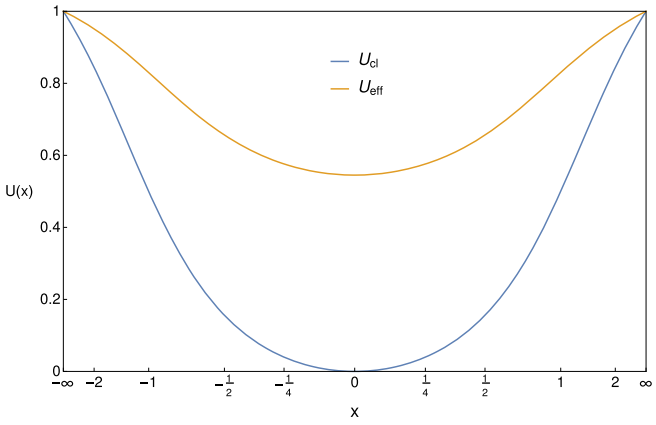

FIG. 9. Comparison of the classical potential (14) and the corresponding effective potential (31) in the large N limit. In contrast to finite N, we do not observe convexity of the effective potential, but only that the ρ derivative is non-negative.

radial mode propagator. In the large N approximation, however, only the equivalent of the Goldstone mode propagator survives, and for it to be finite, it is enough that $U'(\rho) \equiv U'(x)/x$ is non-negative. This is indeed the case for the solution given above. A plot of both the classical and the effective potential is given in Fig. 9.

VI. SUMMARY

We extended the ideas from previous work on functional fixed point equations to also solve functional flow equations to high accuracy. We first discussed flows of the O(N) model in three dimensions, for $N = 1$, 4 and in the large N limit. In all cases, we could achieve a highly stable and precise flow. We showed that our method can accomplish the time integration to machine precision, and always stays very close to the analytical solution exactly known in the large N limit. The error in this case is dominated by the condition of the differential equation. Even for numerically challenging tasks, as resolving the convexity of the effective potential in the IR, the flow was traceable for 6 orders of magnitude for $N = 4$, and about 2 orders of magnitude for $N = 1$. Then, we calculated the flow along a separatrix from the first multicritical fixed point to the Wilson-Fisher fixed point in $d = 2.4$, for which almost 13 orders of magnitude were integrated out at high precision. As a second model, we treated a set of bounded potentials in $d = 1$, which are reminiscent to potentials in a quantum field theory context such as Higgs inflation. Technically, they are interesting because they need global resolution for a numerically stable flow. For the three potentials that we discussed, we extracted the ground state and first excited state energies in a LPA truncation to satisfying accuracy, even though one might have expected from analytic arguments that the determination of the first excited state energy was not possible from the effective potential alone. Finally, nonanalyticities also pose no problem to our method, in contrast to expansions in powers of the field.

ACKNOWLEDGMENTS

We would like to thank A. Bonnano, H. Gies, and A. Wipf for the useful discussions and H. Gies and A. Wipf for the valuable comments on the manuscript. This work was supported by the DFG Research Training Group "Quantum and Gravitational Fields" GRK 1523/2. J. B. acknowledges further support from DFG under Grant No. Gi 328/6-2 (FOR 723), while B. K. is grateful for funding from DFG Grant No. Wi 777/11-1.

[1] C. Wetterich, Phys. Lett. B **301**, 90 (1993).
[2] N. Tetradis and C. Wetterich, Nucl. Phys. **B422**, 541 (1994).
[3] J. Berges, N. Tetradis, and C. Wetterich, Phys. Rep. **363**, 223 (2002).
[4] B. Delamotte, Lect. Notes Phys. **852**, 49 (2012).
[5] T. R. Morris and M. D. Turner, Nucl. Phys. **B509**, 637 (1998).
[6] C. Bervillier, A. Juttner, and D. F. Litim, Nucl. Phys. **B783**, 213 (2007).
[7] D. F. Litim and D. Zappala, Phys. Rev. D **83**, 085009 (2011).
[8] F. Benitez, J.-P. Blaizot, H. Chate, B. Delamotte, R. Mendez-Galain, and N. Wschebor, Phys. Rev. E **85**, 026707 (2012).
[9] A. Codello and G. D'Odorico, Phys. Rev. Lett. **110**, 141601 (2013).
[10] P. Mati, Phys. Rev. D **91**, 125038 (2015).
[11] R. Percacci and G. P. Vacca, Phys. Rev. D **90**, 107702 (2014).
[12] N. Defenu, P. Mati, I. G. Marian, I. Nandori, and A. Trombettoni, J. High Energy Phys. 05 (2015) 141.
[13] A. Codello, N. Defenu, and G. D'Odorico, Phys. Rev. D **91**, 105003 (2015).
[14] P. Mati, arXiv:1601.00450.
[15] T. Hellwig, A. Wipf, and O. Zanusso, Phys. Rev. D **92**, 085027 (2015).
[16] W. Metzner, M. Salmhofer, C. Honerkamp, V. Meden, and K. Schonhammer, Rev. Mod. Phys. **84**, 299 (2012).
[17] M. M. Scherer, S. Floerchinger, and H. Gies, Phil. Trans. R. Soc. A **369**, 2779 (2011).
[18] H. Gies and L. Janssen, Phys. Rev. D **82**, 085018 (2010).

[19] J. Braun, H. Gies, and D. D. Scherer, Phys. Rev. D **83**, 085012 (2011).
[20] J. Braun, J. Phys. G **39**, 033001 (2012).
[21] H. Gies and R. Sondenheimer, Eur. Phys. J. C **75**, 68 (2015).
[22] I. Boettcher, J. M. Pawlowski, and C. Wetterich, Phys. Rev. A **89**, 053630 (2014).
[23] P. Kopietz, L. Bartosch, and F. Schutz, Lect. Notes Phys. **798**, 1 (2010).
[24] L. Janssen and H. Gies, Phys. Rev. D **86**, 105007 (2012).
[25] H. Gies, L. Janssen, S. Rechenberger, and M. M. Scherer, Phys. Rev. D **81**, 025009 (2010).
[26] D. D. Scherer, J. Braun, and H. Gies, J. Phys. A **46**, 285002 (2013).
[27] D. F. Litim, Nucl. Phys. **B631**, 128 (2002).
[28] F. Benitez, J.-P. Blaizot, H. Chate, B. Delamotte, R. Mendez-Galain, and N. Wschebor, Phys. Rev. E **80**, 030103 (2009).
[29] P. Jakubczyk, N. Dupuis, and B. Delamotte, Phys. Rev. E **90**, 062105 (2014).
[30] M. Reuter and C. Wetterich, Nucl. Phys. **B417**, 181 (1994).
[31] H. Gies, Lect. Notes Phys. **852**, 287 (2012).
[32] J. M. Pawlowski, Ann. Phys. (Berlin) **322**, 2831 (2007).
[33] D. F. Litim and J. M. Pawlowski, Phys. Lett. B **435**, 181 (1998).
[34] J. Braun, B. Klein, and B.-J. Schaefer, Phys. Lett. B **713**, 216 (2012).
[35] R.-A. Tripolt, J. Braun, B. Klein, and B.-J. Schaefer, Phys. Rev. D **90**, 054012 (2014).
[36] J. Braun, L. Fister, J. M. Pawlowski, and F. Rennecke, arXiv:1412.1045.
[37] M. Mitter, J. M. Pawlowski, and N. Strodthoff, Phys. Rev. D **91**, 054035 (2015).
[38] M. Reuter, Phys. Rev. D **57**, 971 (1998).
[39] M. Niedermaier and M. Reuter, Living Rev. Relativ. **9**, 5 (2006).
[40] R. Percacci, in *Approaches to Quantum Gravity: Toward a New Understanding of Space, Time and Matter*, edited by D. Oriti (Cambridge University Press, Cambridge, England, 2009), p. 111.
[41] E. Manrique and M. Reuter, Ann. Phys. (Berlin) **325**, 785 (2010).
[42] D. Benedetti, K. Groh, P. F. Machado, and F. Saueressig, J. High Energy Phys. 06 (2011) 079.
[43] D. Benedetti and F. Caravelli, J. High Energy Phys. 06 (2012) 017.
[44] A. Eichhorn, J. High Energy Phys. 04 (2015) 096.
[45] M. Demmel, F. Saueressig, and O. Zanusso, Ann. Phys. (Berlin) **359**, 141 (2015).
[46] N. Christiansen, D. F. Litim, J. M. Pawlowski, and A. Rodigast, Phys. Lett. B **728**, 114 (2014).
[47] K. Falls, D. F. Litim, K. Nikolakopoulos, and C. Rahmede, arXiv:1301.4191.
[48] N. Christiansen, B. Knorr, J. M. Pawlowski, and A. Rodigast, Phys. Rev. D **93**, 044036 (2016).
[49] S. Folkerts, D. F. Litim, and J. M. Pawlowski, Phys. Lett. B **709**, 234 (2012).
[50] A. Eichhorn and H. Gies, New J. Phys. **13**, 125012 (2011).
[51] U. Harst and M. Reuter, J. High Energy Phys. 05 (2011) 119.
[52] P. Donà, A. Eichhorn, and R. Percacci, Phys. Rev. D **89**, 084035 (2014).
[53] R. Percacci and G. P. Vacca, Eur. Phys. J. C **75**, 188 (2015).
[54] H. Gies, B. Knorr, and S. Lippoldt, Phys. Rev. D **92**, 084020 (2015).
[55] N. Christiansen, B. Knorr, J. Meibohm, J. M. Pawlowski, and M. Reichert, Phys. Rev. D **92**, 121501 (2015).
[56] J. Meibohm, J. M. Pawlowski, and M. Reichert, Phys. Rev. D **93**, 084035 (2016).
[57] H. Gies, B. Knorr, S. Lippoldt, and F. Saueressig, Phys. Rev. Lett. **116**, 211302 (2016).
[58] J. Meibohm and J. M. Pawlowski, Eur. Phys. J. C **76**, 285 (2016).
[59] J. Borchardt and B. Knorr, Phys. Rev. D **91**, 105011 (2015).
[60] M. Heilmann, T. Hellwig, B. Knorr, M. Ansorg, and A. Wipf, J. High Energy Phys. 02 (2015) 109.
[61] J. Borchardt, H. Gies, and R. Sondenheimer, arXiv: 1603.05861.
[62] J. P. Boyd, *Chebyshev and Fourier Spectral Methods*, 2nd ed. (Dover Publications, New York, 2000).
[63] R. E. Robson and A. Prytz, Aust. J. Phys. **46**, 465 (1993).
[64] M. Ansorg, A. Kleinwachter, and R. Meinel, Astron. Astrophys. **405**, 711 (2003).
[65] R. P. Macedo and M. Ansorg, J. Comput. Phys. **276**, 357 (2014).
[66] D. F. Litim and L. Vergara, Phys. Lett. B **581**, 263 (2004).
[67] C. S. Fischer and H. Gies, J. High Energy Phys. 10 (2004) 048.
[68] C. Gneiting, Diploma thesis, University of Heidelberg, 2005.
[69] D. Zappala, Phys. Rev. D **86**, 125003 (2012).
[70] S. Grozdanov, D. Kraljic, and E. E. Svanes, Nucl. Phys. **B909**, 657 (2016).
[71] J. Berges and C. Wetterich, Nucl. Phys. **B487**, 675 (1997).
[72] J. Adams, N. Tetradis, J. Berges, F. Freire, C. Wetterich, and S. Bornholdt, Mod. Phys. Lett. A **10**, 2367 (1995).
[73] G. Papp, B. J. Schaefer, H. J. Pirner, and J. Wambach, Phys. Rev. D **61**, 096002 (2000).
[74] O. Bohr, B. J. Schaefer, and J. Wambach, Int. J. Mod. Phys. A **16**, 3823 (2001).
[75] B.-J. Schaefer and J. Wambach, Nucl. Phys. **A757**, 479 (2005).
[76] A. Bonanno and G. Lacagnina, Nucl. Phys. **B693**, 36 (2004).
[77] J.-M. Caillol, Nucl. Phys. **B855**, 854 (2012).
[78] D. Roscher, J. Braun, and J. E. Drut, Phys. Rev. A **91**, 053611 (2015).
[79] I. Boettcher, J. Braun, T. K. Herbst, J. M. Pawlowski, D. Roscher, and C. Wetterich, Phys. Rev. A **91**, 013610 (2015).
[80] T. Fischbacher and F. Synatschke-Czerwonka, Comput. Phys. Commun. **184**, 1931 (2013).
[81] F. Synatschke-Czerwonka, T. Fischbacher, and G. Bergner, Phys. Rev. D **82**, 085003 (2010).
[82] M. Mitter and B.-J. Schaefer, Phys. Rev. D **89**, 054027 (2014).
[83] N. Strodthoff, B.-J. Schaefer, and L. von Smekal, Phys. Rev. D **85**, 074007 (2012).
[84] T. K. Herbst, M. Mitter, J. M. Pawlowski, B.-J. Schaefer, and R. Stiele, Phys. Lett. B **731**, 248 (2014).

[85] M. Peláez and N. Wschebor, arXiv:1510.05709.
[86] BOOST C++ libraries 1.57.0, 2014, http://www.boost.org.
[87] G. Guennebaud, B. Jacob *et al.*, http://eigen.tuxfamily.org.
[88] The BLITZ++ metatemplate library, 2015, http://blitz.sourceforge.net/.
[89] H. Wang and S. Xiang, Math. Comput. **81**, 861 (2012).
[90] In [59] we used rational Chebyshev functions to resolve the asymptotic part. From the point of view of an implementation in an actual code, it is more convenient to work with a compactification as presented here. This does not have any impact on convergence, so any choice made is purely conventional.
[91] W. Guo, G. Labrosse, and R. Narayanan, *Lecture Notes in Applied and Computational Mechanics* Vol. 68 (Springer, New York, 2013).
[92] N. Tetradis and D. F. Litim, Nucl. Phys. **B464**, 492 (1996).
[93] E. Ising, Z. Phys. **31**, 253 (1925).
[94] L. Onsager, Phys. Rev. **65**, 117 (1944).
[95] A. Hasenfratz and P. Hasenfratz, Nucl. Phys. **B270**, 687 (1986).
[96] Here, we use the Goldstone anomalous dimension, even for $N = 1$, as this leads to superior results.
[97] D. F. Litim, Phys. Rev. D **64**, 105007 (2001).
[98] D. F. Litim, Phys. Lett. B **486**, 92 (2000).
[99] D. F. Litim, J. M. Pawlowski, and L. Vergara, arXiv:hep-th/0602140.
[100] A. Codello, J. Phys. A **45**, 465006 (2012).
[101] I. D. Saltas, J. Cosmol. Astropart. Phys. 02 (2016) 048.
[102] G. Pöschl and E. Teller, Z. Phys. **83**, 143 (1933).
[103] Y. Fujimoto, L. O'Raifeartaigh, and G. Parravicini, Nucl. Phys. **B212**, 268 (1983).
[104] S. R. Coleman and E. J. Weinberg, Phys. Rev. D **7**, 1888 (1973).
[105] T. L. Curtright and C. B. Thorn, J. Math. Phys. (N.Y.) **25**, 541 (1984).
[106] S. Coleman, *Aspects of Symmetry* (Cambridge University Press, Cambridge, England, 1985).
[107] K. Symanzik, Commun. Math. Phys. **16**, 48 (1970).
[108] P. M. Stevenson, Phys. Rev. D **30**, 1712 (1984).
[109] A. S. Kapoyannis and N. Tetradis, Phys. Lett. A **276**, 225 (2000).